WARSAW UNIVERSITY OF TECHNOLOGY Index 351733
FACULTY OF CIVIL ENGINEERING
COMMITTEE FOR CIVIL AND WATER ENGINEERING
POLISH ACADEMY OF SCIENCES ISSN 1230-2945
DOI: 10.24425/ace.2024.150969
ARCHIVES OF CIVIL ENGINEERING
Vol. LXX ISSUE 3 2024
pp. 39 –55

Research paper

Long-term SHM (Structural Health Monitoring) of continuous rigid frame bridge reinforced by external prestressing

Xilong Zheng[1]

Abstract: The SHM (Structural Health Monitoring) system deployed for an external prestressing tendon and steel plates rehabilitated continuous rigid frame bridge is introduced in this paper. Damages and deterioration of the large box girder was described as well as the rehabilitation plan. Data that were collected for 6 monthes were analyzed. Performance of the rehabilitated bridge, pattern of the collected data as well as investigation of the correlation between different types of data were the research focus. Temperature was considered as a major issue in the monitored data, the effort has been made to eliminate the effect of temperature in deformation and strain data. The best outlier detection method for deformation data is determined to be IQR analysis, for strain data a thresholding method of the empirical value 200 με was used, and lastly for tension force a thresholding method of 85% tension force was determined to be the best and most reasonable for outlier removal. The variation range of deflection and strain can help determine whether the vehicle load is over the limit.

Keywords: continuous rigid frame bridge, rehabilitation, long-term monitoring, external prestressing tendon

[1]PhD., Harbin University, School of Civil and Architectural Engineering, No.109 Zhongxing Da Dao, Harbin, China, e-mail: sampson88@126.com, ORCID: 0000-0001-5571-667X

1. Introduction

Bridges, amid different types of civil infrastructure, play a key role in the transportation infrastructure that has a considerable impact on long-term economic growth and productivity [1–5]. Frequent health inspection and evaluation at a regular time period are mandatory for maintaining the ultimate purpose of bridges, to provide passage over obstacles and other otherwise inconvenient structures [6–9].

Traditional non-destructive evaluation (NDE) is practiced by qualified trained inspector on-site using visual inspection and technical equipments [10–12]. However, the quality of accessment depends highly on the precision and accuracy of the equipments and the experience and judgment of the inspecters. The condition of the bridge can only be determined in the presence of inspectors [13, 14]. As a result, there is a constant concern of the occurrence of serious damages between inspection periods. A notable example is the failure of ashtabula. Investigation showed that this failure resulted from buckling and fracture of critical members due to the lack of inspection and maintenance [15].

Structural Health monitoring (SHM) is an extension and improvement of nondestructive testing techniques, which install sensors on the intended structure to enable continuous detection and evaluation of the structure's condition [16, 17]. Moreover, these monitored data are recorded and can be used to analyze and predict structure deteriorations. While most bridge health monitoring systems are installed on newly constructed bridges, rehabilitated bridges are rarely being monitored, not to mention external prestressing strengthened continuous rigid frame bridges. Therefore, it is necessary to study the health monitoring of the repaired bridge.

SHM system consists of two functioning sub-systems, the data monitoring system and the data processing and analysis system [18–20]. The data monitoring sub-system consists of sensor networks and data collection and transmission. Furthermore, continuous monitoring offers mean to catch the deficiencies at first appearance, rather than at the next inspection cycle, allowing for repair before the damage has an opportunity to cause further deterioration to the system [21]. By complementing the current inspection process, it provides bridge managers with more information about current capabilities and rates of structural degradation so that they can more accurately predict future maintenance needs.

2. Background bridge overview

The rehabilitated highway bridge located in the northeast region of China, first opened to traffic in December 2010. The bridge has a total length of 549356 mm, and a total width of 24.5 m. The bridge is 12 m in width with 2 traffic lanes. The span arrangement is 75 m + 3 × 130 m + 75 m, as shown in Fig. 1 and Fig. 2.

Fig. 1. General view of the rehabilated highway bridge

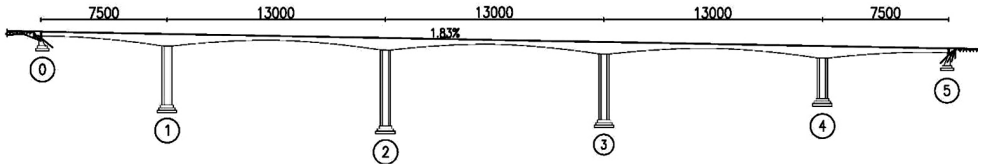

Fig. 2. General view of the rehabilitated highway bridge (unit: cm)

2.1. Original bridge design

1. Superstructure
   The superstructure consists of a three-span continuous prestressed concrete large box girder. The box girder is single-walled. 7.0 m in height being the tallest cross-section on top of a pier, whereas 2.5 m in height at mid-span. The bottom slab of the box girder is 5.6 m in width, and the flange of the bridge is 3.2 m in width.
   The top slab of the box girder is 0.25 m in thickness, and 0.50 m in thickness for cross-sections near a pier. The thickness of the web is 0.8 m around a pier, 0.40 m for the 81.4 m range in the middle of the span, and 0.6 m for the rest of the web. The thickness of the bottom slab on top of a pier is 1.2 m, 1.0 m at the pier junction, 0.25 m at mid-span. An illustration of typical cross-sections is shown in Fig. 3.

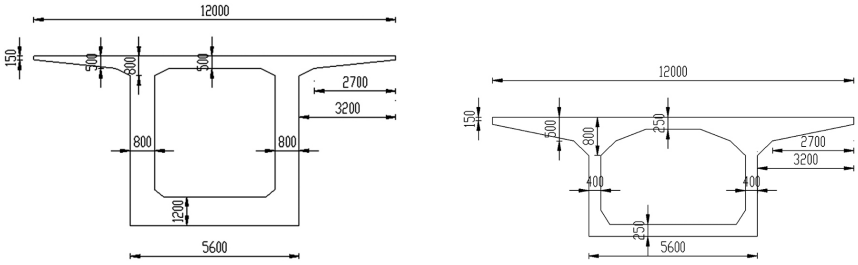

Fig. 3. Cross-section view: (a) Top of a pier (b) Mid-span (unit: mm)

2. Design load
   The bridge was designed according to the old specification of JTG 021-1985 “General Code for the Design of Highway Bridges and Culverts”. During retrofit design, newer specification, JTG D60-2004 “General Code for the Design of Highway Bridges and Culverts” was used, and aiming for a design life of 20 years.

2.2. Bridge damages and deteriorations

The particular rigid frame continuous box girder bridge of interest in this study was first opened to traffic in 2006. However, after as little as 6 years of operation, the bridge showed signs of deterioration and decreased the bearing capacity. During routine inspections in 2012, 2013 and 2015, cracks were observed on the top slab, web slab and bottom slab, more severe on the exterior surfaces than the interior. The length, width and number of cracks were growing with passage of time. Most of the cracks were between 0.15 mm ~ 0.4 mm in width and 0.3 m ~ 7 m in length. According to the codes and specifications, the prestressed concrete beams are not allowed to have cross-sectional cracks, and the allowable width of longitudinal cracks is 0.2 mm. The width of some longitudinal cracks on the box girder exceeds the specified value.

In 2012, routine inspection was conducted. The inner surface of the web has 8 oblique cracks on the left, with a total length of 29.5 m, and 13 oblique cracks on the right, with a total length of 41.2 m. The outside surface of the web has cracks mainly concentrated in the blocks 7 ~ 9, about 10 counts with a total length of 42.6 m, 4 oblique cracks on the left side with a total length of 13.2 m, and 6 oblique cracks on the right side with a total length of 29.41 m. The cracks were distributed along the directions of 20° and 45°, width was generally between 0.2 mm and 0.5 mm.

In 2013 and 2015, the routine inspection was conducted again, cracks distribution was similar compared to the inspection in 2012. However, cracks on the web gradually developed into transverse cracks at the chamfering angle of the top slab. As a result, a total of 156 oblique cracks were detected on the web of the box girder, with a total length of 38.6 m, among which 72 cracks on the right side with a total length of 19.3 m and 84 cracks on the left side with a total length of 19.3 m. Crack distribution on the web of the box girder is shown in Fig. 4.

(a) (b)

Fig. 4. Cracks distribution on the web: (a) Crack on the No. 8 block exterior surface (L = 4 m, δ = 0.5 mm, α = 45°); (b) Interior surface oblique crack (L = 8 m, δ = 0.5 mm, α = 35°)

The web of the bridge is seriously cracked, and the distribution range of the inner cracks of the web is from 6 # block to 14 # block. The lateral cracks of the web were mainly concentrated in blocks 7 # to 9 #, while no cracks appeared in blocks 0 # to 5 #. After checking the bridge design drawings, the thickness of the web of blocks 0 # ~ 5 # is 60 cm, and prestressed steel bundles are arranged, while the thickness of the web of blocks 6 # ~ 14 # is 40 cm, and there is no prestressed steel bundles, and the diameter of the web stirrings is 10 mm. Through calculation and analysis, the web size of 7 # ~ 9 # blocks does not meet the requirements of minimum shear size. It can be seen that the inclined crack of the web is caused by the joint action of bending moment and shear force, and is caused by excessive main tensile stress.

Through calculation and analysis, the shear strength and crack resistance of the top slab meet the requirements of the code. The transverse and longitudinal prestressed steel bundles are arranged in the top slab with a thin thickness of 25 cm. The longitudinal steel bundles are close to the lower edge of the top slab and are easy to form cracks along the longitudinal steel bundles. The crack of the bottom slab is caused by excessive prestressed radial force and insufficient reinforcement. In addition, the uneven positioning of prestressed steel bundles during construction is also the cause of cracks in the bottom slab.

In the 2013 inspection, five longitudinal cracks were observed at the exterior surface of the fold section bottom slab of span No. 2, with the length of cracks ranging from 2 m to 7 m and the width ranging from 0.6 mm to 4 mm. In the 2015 inspection, 9 longitudinal cracks were found on the bottom slab of the fold section. Four longitudinal cracks on the bottom slab and seven longitudinal cracks were found in the No. 3 span. whereas No. 2 span bottom slab was the most severe, with a maximum width of 4 mm and a depth of 3 mm, accompanied by concrete separation. After chipping away loose concrete around the crack, the prestressed strand was found and the corrugate pipe was slightly damaged. Damages are shown in Fig. 5.

(a) (b)

Fig. 5. Cracks on the bottom slab of the box girder: (a) Span No. 2 longitudinal crack corrugate pipe deterioration; (b) Span No.2 Longitudinal crack hollow section

The number, length, and width of cracks increase with the number of years of operation as shown in Fig. 6. From 2012 to 2013, the width of cracks on the web increased by 24.77%, and the number of cracks increased by 103, and the length increased by 229.37 m. From 2013 to 2015, the width of cracks increased by 11.26%, the number of cracks increased by 60, and the length increased by 163.03 m.

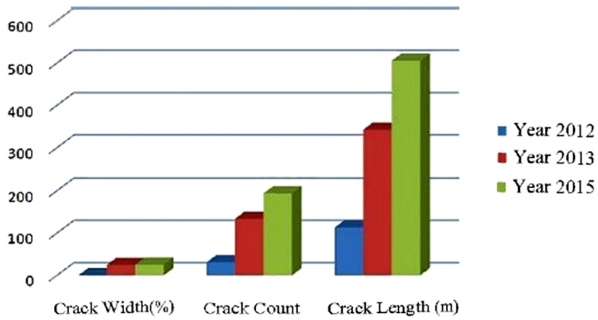

Fig. 6. Cracks profile over 3 inspection periods

2.3. Rehabilitation with external prestressing and steel plates

1. External Prestressing Strengthening
   External prestressing strands were anchored on the inner surface of the box girder, 8 external tendons for each span. Detailed arrangements are shown in Fig. 7 to Fig. 9. Six prestressed steel bundles are used on both sides of the span, and eight prestressed steel bundles are used on the three middle span. Each steel bundle consists of 15 prestressed steel strands with a nominal diameter of 15.2 mm. Considering the fatigue of external prestressed steel strand, the tensile control stress of external prestressed steel strand is 930 MPa. External prestressing can reduce the web shear force, so that the main tensile stress of the web can meet the requirements, and can improve the bearing capacity of the main beam.

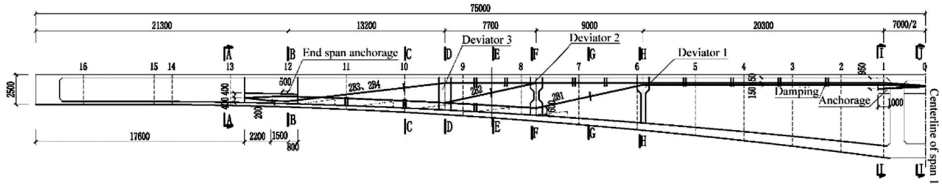

Fig. 7. External prestressing strands arrangements for end span, side span, and middle span (unit: mm)

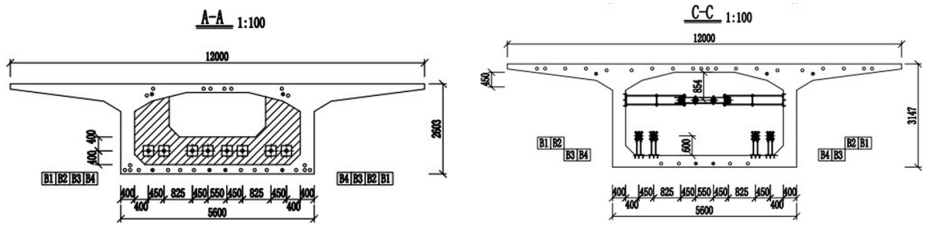

(a) (b)

Fig. 8. Cross section view of external prestressings: (a) Section A–A; (b) Section B–B

Fig. 9. On-site installation of external prestressing tendon

Fig. 10. Steel plates on the interior of the girder web

2. Oblique cracks strengthening
   Reinforcement stirrups of the web slab are of diameter Φ10, which are not sufficient in restricting crack growth. Therefore, steel plates of grade Q235C were pasted on sections 6 ~ 14 inside the girder and on sections 6 ~ 10 outside the girder to limit diagonal cross-section strength. The size of the steel plates is 60 mm wide and 6 mm thick, length depends on the height of the web, 150 mm spacing on the inside and 200 mm spacing on the outside. The anticorrosive coating used zinc-rich primer plus coal tar epoxy coating. Two layers of zinc-rich primer, each of 35 μm, and two layers of coal tar epoxy coating, 80 μm and 120 μm. The total thickness of the steel plate is 200 μm as shown in Fig. 10. For severe diagonal cracks that existed, they should be sealed before steel plates pasting.
3. Top slab strengthening and seepage control
   The top slab strengthening adopts steel plate pasting on the lower edge of the top slab in order to improve the anti-crack ability of the top slab. According to the routine inspection report, cracks in the top slab appear in the un-thickened areas of the web. The thickened area of the web reduced the span of the bridge deck, so it is advantageous for structural mechanics. Therefore, the steel plate strengthening range is the un-thickened area of the web. Before steel plate pasting, cementation of the cracks was performed on the interior of the top slab using NSF fine aggregate concrete, then steel plates of grade Q235C steel were pasted with 200 mm spacing. The size of the steel plates is $L \times 60 \times 6$ mm^3, where, L is the cross-sectional length of the top slab interior as shown in Fig. 11.

(a)

(b)

Fig. 11. Steel plates on the interior of the girder top slab: (a) A perspective; (b) Another perspective

Seepage control was accomplished by re-doing the water-proof layer and the pavement of bridge deck, optimization of road surface water drainage to prevent any leakage.

3. Structural health monitoring program

Based on the characteristics of the rehabilitated bridge, the damage sensitive parameter such as bridge deck curvature and structural mechanics behaviors are the main objectives of this instrumentation design.

The SHM system consists of two major components, the DA system and sensors. The DA system includes a centralized data acquisition module, general data acquisition module JMZX-32A, solar power, sim card and signal emitter, and the sensor netwok includes strain gauges, pressure cells, and tiltmeters. These sensors are responsible for the measurements of strain, deflection and tension of the external tendons.

The overall setup of the three different types of sensors is shown in Fig. 12, a total of 14 sensors were instrumented.

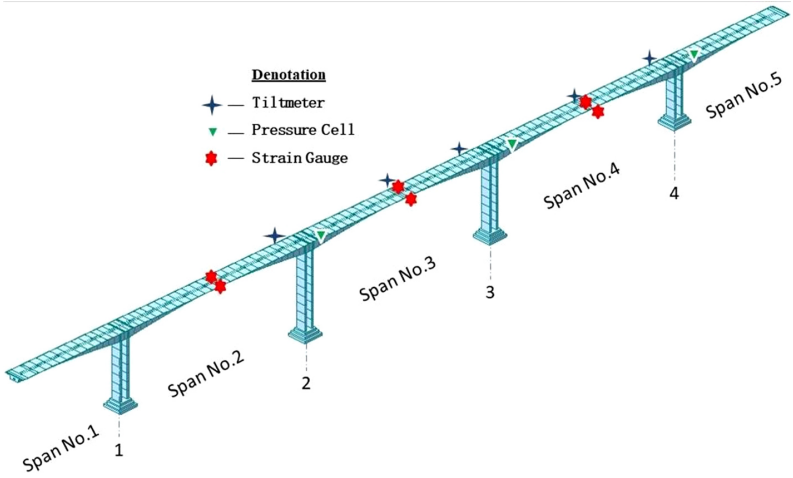

Fig. 12. Illustration of overall sensor locations

3.1. Deck curvature measurement

Change in bridge deck curvature is a significant indicator of bridge health, especially deflection for rigid frame bridges. Deformation in structures can be divided into two categories: global deformation and local deformation. Global deformations are directly reflected in the serviceability of the structure. Whereas, local deformations are reflected in the deformation of each structural component. Therefore, monitoring of deck curvature is crutial in bridge health evaluation.

There are two main methods of curvature measurement. Traditional methods of using dial gauges or deflectometers are not suitable for long-term monitoring. The SHM system sensors installed in the structure enable long-term continuous monitoring.

Tiltmeters that are installed on-site are shown in Fig. 13 below. The tiltmeter were installed on the web of the interior surface of the girder at midspan, and installed on the bottom slab of the girder near piers so that the tiltmeters are at the same elevation.

(a) (b)

Fig. 13. Deck curvature measurement point: (a) Tiltmeter installed at midspan; (b) Tiltmeter installed near the pier

3.2. Strain measurement

JMZX-212HAT vibrating wire strain gauges, which are a component of the JMZX-21A general data acquisition module, are used to measure strain response and it is also equipped with temperature sensors. The vibrating wire strain gauge consists of a vibrating tensioned wire, base, strain gauge, and protecting cover, suitable for steel structure and concrete structure surface strain measurements. The base of the strain gauge is welded onto the steel structure or nailed by high-strength bolt into the surface of the concrete, and is commonly used for long-term and automated measurement. The strain is calculated by measuring the resonant frequency of the wire (an increase in tension increases the resonant frequency).

On-site installation of JMZX-212HAT Surface Strain Gauge and an illustration of the box-girder instrumentation cross-section is shown in Fig. 14.

(a) (b)

Fig. 14. On-site installation of surface strain gauges: (a) Top slab; (b) Bottom slab

3.3. External tendon tension measurement

JMZX-3330AT pressure cell is a hollowed multi-string pressure sensor, also called pressure cell, which is suitable for tension force measurement such as tensioned prestressing force, and tension force while stretching. Since temperature sensors are also embedded, JMZX-3330AT pressure cell is capable of automatic temperature correction of the measured pressure value. On-site pressure cell installation on the anchorage is shown in Fig. 15.

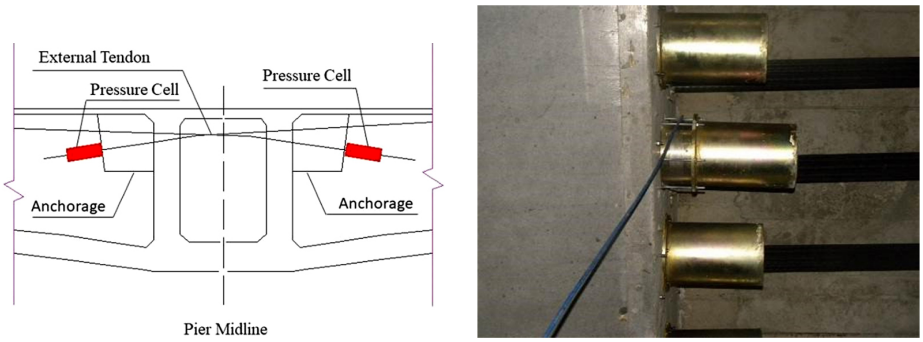

(a) (b)

Fig. 15. On-site pressure cell installation on the anchorage: (a) Schematic diagram; (b) Cable gauge picture

Data collected through above mentioned sensors are centralized at the data acquisition modules, as shown in Fig. 16, these raw data are then transferred via a GPRS wireless communication network or telecommunication network to the database and archived.

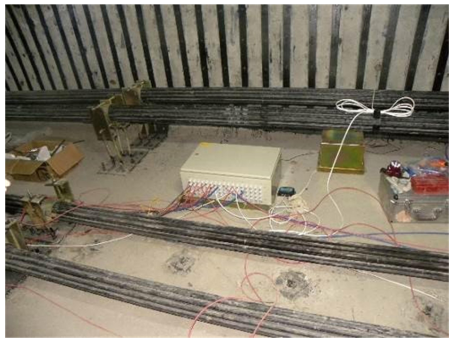

Fig. 16. Acquisition and wireless data transfer module on-site

Real-time monitored data is visible through the user interface as shown in Fig. 16. In the user interface, all parameters of the real-time monitored data such as date, time, module number, channel number, sensor type, sensor number, data value and its unit, electrical resistance, and temperature can be visualized.

4. Pattern analysis of long-term health monitoring data

4.1. Key cross-section deflection data

Deflection data collected from the five sensor locations at span 3 midspan, span 4 midspan, pier 2, pier 3, and pier 4 for the last 6 months of 2018 are shown in Fig. 17 below.

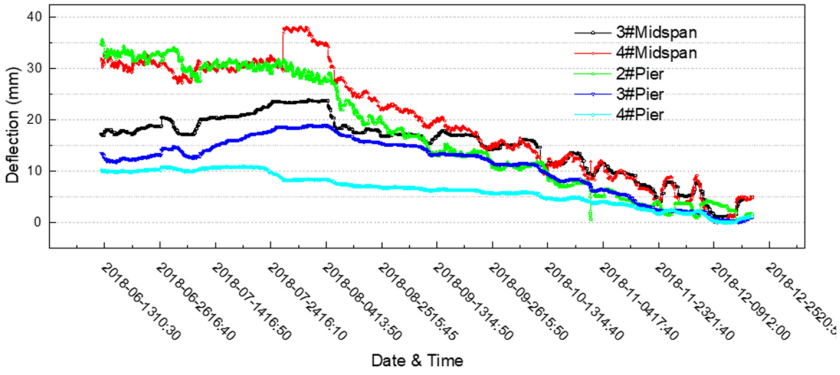

Fig. 17. Deflection change monitored for the last 6 months of 2018

Overall an increasing trend is observed starting from June 10th to the end of July, where deflection change reached maximum. Deflection change then showed a decreasing trend since that time until December 21st.

At span 3 midspan, the relative deflection change is within 22.75 mm. Maximum value is observed on July 26th and minimum value is observed on December 10th. Peak is observed around the maximum value around the end of July.

At span 4 midspan, the total change in deflection over the last 6 months of 2018 is around 38.18 mm. Span 4 midspan showed a significant peak around the end of July, maximum value is observed at July 29 th 15:40. and minimum value is observed at December 10 th 9:10.

Pier 2 has shown a similar increasing and decreasing trend as span 3 midspan and span 4 midspan. The total deflection change is 35.67 mm, the maximum occurred at 17:00 on December 16.

Pier 3 deflection data peak is also observed at the end of July and minimum is observed at December 17th, which is similar as the trend observed for midspan deflections. The total deflection change is 19.05 mm.

Pier 4 has shown a steady decreasing trend in overall. Total deflection change is as little as 10.86 mm. Maximum value is observed on July 2nd, and minimum value is observed on December 12th.

As shown in Fig. 18, temperature increased from June to the end of July and decreased until the end of December in general. Deflection has showed a similar trend as temperature. Maximum temperature of span 2 midspan top slab measured was 33.4° on July 27 and minimum temperature was –15.8° on November 21. Maximum temperature of span 3 midspan bottom slab measured was 30.6° on July 27 and minimum temperature is –16.2° on November 21st

from 02:00h to 03:50 h. Maximum temperature of span 4 midspan bottom slab measured is 29.3° on July 27th from 10:30 h to 11:00 h and minimum temperature is –16.9° on November 21st 04:20 h. To summarize, temperature data measured from all sensors are fairly consistent. On July 26th or 27th, the temperature is the highest and November 21st, 26th or 27th being the lowest temperature of the last 6 months of 2018.

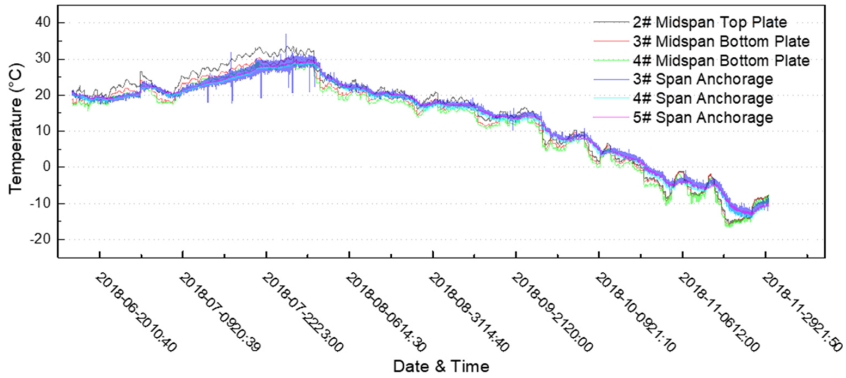

Fig. 18. Temperature data monitored for the last 6 months of 2018

4.1.1. Temperature effect removal

The portion of the data from June 10th to July 10th, as shown in Fig. 19, was extracted for demonstration analysis. In order to remove the temperature effect, temperature is used as an independent variable to simulate deflection caused by temperature, as shown in Fig. 20. Linear regression has an $R2$ of 0.54. To verify using F value, $F = 2257.11 > F0.05$, and its corresponding $p > 0$, which satisfies $p < 0.05$. Therefore, there is indeed a high correlation between temperature and deflection. It makes sense to use this method for temperature effect simulation.

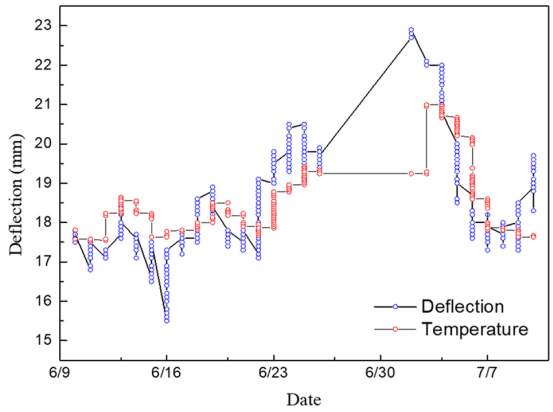

Fig. 19. Temperature and deflection from June 10th to July 10^{th}

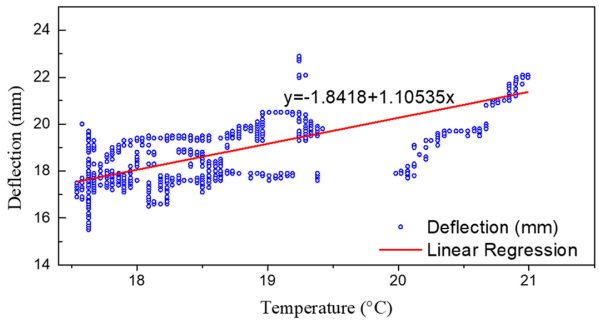

Fig. 20. Temperature and deflection correlation and linear regression

Total deflection subtracts linear regression simulated data would be the result. The resulting deflection calculated from the linear regression model and temperature data is shown in Fig. 21. The change in deflection can now be seen as the deflection caused by vehicle load alone.

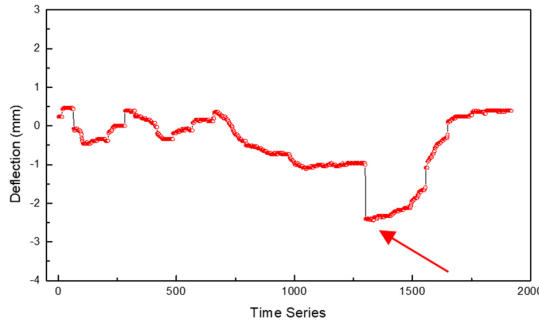

Fig. 21. Deflection after the removal of temperature effect

As shown by the arrow, continuous heavy traffic flow was observed at the range of [1302, 1509] for a total of 207 minutes or 34.5 hours. However, there should be unloading during this period which was not observed. This leads to two explanations to this phenomenon, one is that there was indeed continuous heavy traffic flow during that period or there were intervals of traffic flow. To verify this, strain responses during the same time series range will be analyzed for consistency.

4.2. Top and bottom slab strain at midspan

Under normal operating conditions, the strain caused by dead load can be treated as a constant value. Strain caused by concrete shrinkage and creep decreases on at an exponential rate, where 75% of the changes occurred within the first year and the remaining 25% within 20 years. This value can be calculated and removed. Through the research conducted, after three years of bridge erection, shrinkage and creep change will reach a plateau and its effect can be ignored. In this case, the SHM system was installed long after three years of bridge erection. The main cause of effect to consider would be temperature.

Top slab and bottom slab strains are analyzed separately, since the top slab of the midspan are mainly under compression and the bottom slab are mainly tension members.

Strain data for the last 6 months of 2018 at the midspan is shown in Fig. 22. As shown by Fig. 22(a), span 3 midspan has show a slightly different trend than the other top slab strains. Relative strain changes for span 2 midspan top slab is 181.3 με, for span 3 mid-span is 179.9 με, and for span 4 midspan is 159.15 με.

As shown by Fig. 22(b), Strain of the bottom slab showed remarkably resemblance. Relative strain changes for span 2 midspan is 181.8 με with maximum value of 5.2 on July 13th and minimum value of –176.6 on December 11th; for span 3 midspan relative change is 140.1 με with maximum value of 4 on July 24th and minimum value of –136.1 on December 8th; and relative change for span 3 midspan is 203.6 με with maximum value of 27.4 on July 25th and minimum value of –176.2 on December 8th.

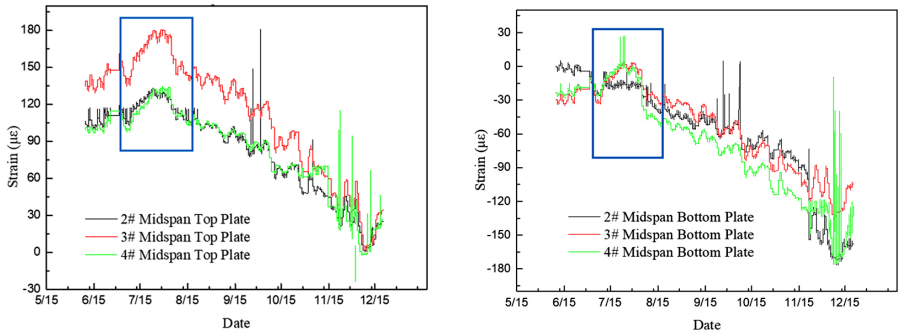

(a) (b)

Fig. 22. Strain data for the last 6 months of 2018 at the midspan: (a) Top slabs, and (b) Bottom slabs

4.3. Temperature effect removal

Used the same algorithm as the treatment of deflection data, the temperature effect of strain data from June 10th to July 10th, were treated. Results are shown in Fig. 23.

Time series data in the range of [1302, 1509] for both top and bottom slab showed dramatic change in strain. This corresponds to the change detected in deflection, indicating the presence of vehicle load. The strain change for the data range of [1302, 1509] is 16.20 με for span 2 midspan bottom slab, 10.60 με for span 3 midspan bottom slab, and 8.70 με for span 4 midspan bottom slab. The strain change for the data range of [1302, 1509] is 10.58 με for span 2 midspan top slab, 18.39 με for span 3 midspan top slab, and 12.42 με for span 4 midspan top slab.

4.4. External tendon tension force

Tension forces of external prestressing tendon has been temperature corrected automatically by pressure cells, data collected for the last 6 monthes of 2018 is shown in Fig. 24. The maximum change of external prestressed steel strand tensile force of the 3rd span, 4th span and 5th span is

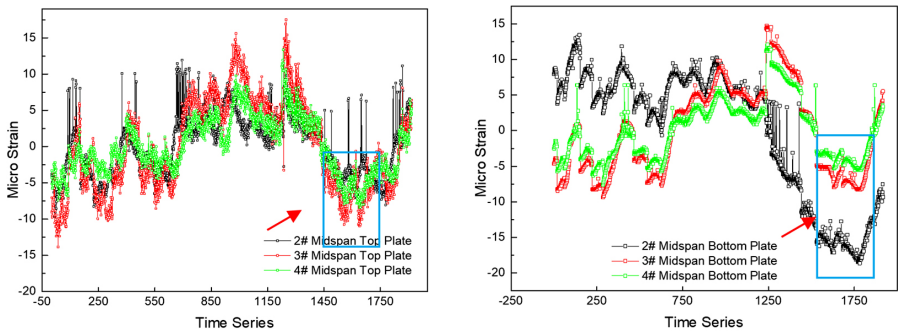

(a) (b)

Fig. 23. Resulting temperature removed strains: (a) Top slabs and (b) Bottom slabs

226 kN, 518 kN and 387 kN, respectively. The peak tensile forces of the 3rd, 4th and 5th span are 1930 kN, 1884 kN and 1952 kN, respectively. Through the evaluation of tension force data, no over-limit data was observed. The rehabilitated bridge has not experienced tension loss.

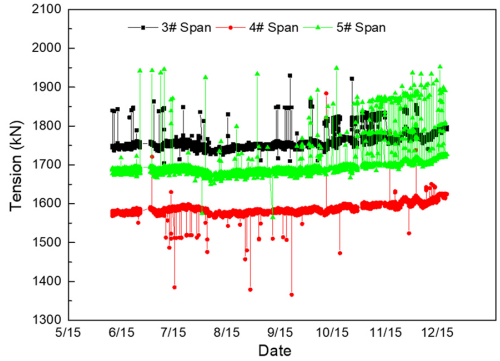

Fig. 24. Tension force data for the last 6 months of 2018

5. Conclusions

1. Data preprocessing was done for the deformation data, strain data and tension force data. Outlier detection methods were compared. The best outlier detection method for deformation data is determined to be IQR analysis, for strain data a thresholding method of the empirical value 200 με was used, and lastly for tension force a thresholding method of 85% tension force was determined to be the best and most reasonable for outlier removal.
2. Over the past six months of 2018, the fourth span has seen the largest change in total deflection, at about 38.18 mm. A significant peak occurred around the end of July, with the maximum occurring at 15:40 on 29 July. The minimum occurred at 9:10 on December 10.

3. The maximum change of external prestressed steel strand tensile force of the 3rd span, 4th span and 5th span is 226 kN, 518 kN and 387 kN, respectively. The peak tensile forces of the 3rd, 4th and 5th span are 1930 kN, 1884 kN and 1952 kN, respectively. Through the evaluation of tension force data, no over-limit data was observed. The rehabilitated bridge has not experienced tension loss.
4. Deformation data and strain data in the time series range of [1302, 1509] has shown related responses, which may help in determining the vehicle load in the future.

References

[1] H. Jia, J. Zhao, X. Li, et al., "Probabilistic pounding analysis of high-pier continuous rigid frame bridge with actual site conditions", *Earthquakes and Structures*, vol. 15, no. 2, pp. 193–202, 2018, doi: 10.12989/eas.2018.15.2.193.

[2] Y. Peng and Z. Zhang, "Development of a novel type of open-web continuous reinforced-concrete rigid-frame bridge", *Journal of Bridge Engineering*, vol. 25, no. 8, art. no. 05020005, 2020, doi: 10.1061/(ASCE)BE.1943-5592.0001595.

[3] S. Ameduri, M. Ciminello, I. Dimino, A. Concilio, A. Catignani, and R. Mancinelli, "Distributed sensor placement optimization for computer aided structural health monitoring", *Archive of Mechanical Engineering*, vol. 66, no. 1, pp. 111–127, 2019, doi: 10.24425/ame.2019.126375.

[4] Z. Zong, Z. Xia, H. Liu, et al., "Collapse failure of prestressed concrete continuous rigid-frame bridge under strong earthquake excitation: Testing and simulation", *Journal of Bridge Engineering*, vol. 21, no. 9, pp. 04016047, 2016, doi: 10.1061/(ASCE)BE.1943-5592.0000912.

[5] M. Fawad, K. Koris, M. Salamak, M. Gerges, L. Bednarski, and R. Sienko, "Nonlinear modelling of a bridge: A case study-based damage evaluation and proposal of Structural Health Monitoring (SHM) system", *Archives of Civil Engineering*, vol. 68, no. 3, pp. 569–584, 2022, doi: 10.24425/ace.2022.141903.

[6] J. Li and L. Xu, "Seismic performance improvement of continuous rigid-frame bridges with hybrid control system under near-fault ground motions", *Soil Dynamics and Earthquake Engineering*, vol. 168, art. no. 107858, 2023, doi: 10.1016/j.soildyn.2023.107858.

[7] M. Yoshikawa, H. Hayashi, S. Kawakita, and M. Hayashida, "Construction of Benten Viaduct, rigid-frame bridge with seismic isolators at the foot ofbpiers", *Cement and Concrete Composites*, vol. 22, no. 1, pp. 39–46, 2000, doi: 10.1016/S0958-9465(99)00047-5.

[8] A. Shan, "Analytical research on deformation monitoring of large span continuous rigid frame bridge during operation", *Engineering*, vol. 7, no. 8, 2015, doi: 10.4236/eng.2015.78044.

[9] K. Wei, J. Zhang, and S. Qin, "Experimental and numerical assessment into frequency domain dynamic response of deep water rigid-frame bridge", *Journal of Earthquake Engineering*, vol. 26, no. 1, pp. 307–330, 2022, doi: 10.1080/13632469.2019.1684402.

[10] L. Wang, D.S. Li, and J.P. Ou, "Fiber bragg grating temperature sensor system on a twin-deck continuous rigid frame bridge for long term monitoring", *Advanced Materials Research*, vol. 148–149, pp. 1611–1618, 2010, doi: 10.4028/www.scientific.net/AMR.148-149.1611.

[11] H.C. Gomez, P.J. Fanning, M.Q. Feng, and S. Lee, "Testing and long-term monitoring of a curved concrete box girder bridge", *Engineering Structures*, vol. 33, no. 10, pp. 2861–2869, 2011, doi: 10.1016/j.engstruct.2011.05.026.

[12] M.R. Nashta, R. Taghipour, M. Bozorgnasab, and H. Mirgolbabaei, "A novel method for identification of damage location in frame structures using a modal parameters-based indicator", *Archives of Civil Engineering*, vol. 68, no. 3, pp. 633–643, 2022, doi: 10.24425/ace.2022.141907.

[13] P. Ryjáček and M. Vokáč, "Long-term monitoring of steel railway bridge interaction with continuous welded rail", *Journal of Constructional Steel Research*, vol. 99, pp. 176–186, 2014, doi: 10.1016/j.jcsr.2014.04.009.

[14] D. Wu and L. Liu, "Study on iterative modification method of parameters in the health monitoring of large-span continuous rigid frame bridges", *Journal of The Institution of Engineers (India): Series A*, vol. 103, no. 1, pp. 271–281, 2022, doi: 10.1007/s40030-021-00613-1.

[15] A. Haidarpour and K.F. Tee, "Finite element model updating for structural health monitoring", *Structural Durability & Health Monitoring*, vol. 14, no. 1, pp. 1-17, 2020, doi: 10.32604/sdhm.2020.08792.

[16] A. Silik, X. Wang, C. Mei, et al., "Development of features for early detection of defects and assessment of bridge decks", *Structural Durability & Health Monitoring*, vol. 17, no. 4, pp. 257–281, 2023, doi: 10.32604/sdhm.2023.023617.

[17] A. Sharma, P. Kumar, H.K. Vinayak, and S.K. Walia, "Condition evaluation in steel truss bridge with fused Hilbert transform, spectral kurtosis, and bandpass filter", *Structural Durability & Health Monitoring*, vol. 15, no. 2, pp. 139–165, 2021, doi: 10.32604/sdhm.2021.012316.

[18] S.S. Pardeshi, A.D. Patange, R. Jegadeeshwaran, and M.R. Bhosale, "Tyre pressure supervision of two wheeler using machine learning", *Structural Durability & Health Monitoring*, vol. 16, no. 3, pp. 271–290, 2022, doi: 10.32604/sdhm.2022.010622.

[19] J.M. Ko and Y.Q. Ni, "Technology developments in structural health monitoring of large-scale bridges", *Engineering Structures*, vol. 27, no. 12, pp. 1715–1725, 2005, doi: 10.1016/j.engstruct.2005.02.021.

[20] K.Y. Koo, J.M.W. Brownjohn, D.I. List, and R. Cole, "Structural health monitoring of the tamar suspension bridge", *Structural Control and Health Monitoring*, vol. 20, no. 4, pp. 609–625, 2013, doi: 10.1002/stc.1481.

[21] D. Reagan, A. Sabato, and C. Niezrecki, "Feasibility of using digital image correlation for unmanned aerial vehicle structural health monitoring of bridges", *Structural Health Monitoring*, vol. 17, no. 5, pp. 1056–107, 2018, doi: 10.1177/1475921717735326.

Received: 2023-10-16, Revised: 2023-12-28